

Cellular Heterogeneity and IL-17 Pathway Dynamics Reveal Insights into the Transition from Ulcerative Colitis to Colorectal Cancer Through scRNA-Seq Analysis

Yaxian Li^{1,*}, Ruochuan Sun^{1,*}, Xiaodong Wang², Mengdi Ma¹, Huizhen Wang¹, Bo Yang¹, Yida Lu³, Yongxiang Li¹

¹Department of General Surgery, First Affiliated Hospital of Anhui Medical University, Hefei, People's Republic of China; ²The Robert Bosch Center for Tumor Diseases (RBCT), Stuttgart, 70376, Germany; ³Department of General Surgery, Second Affiliated Hospital of Anhui Medical University, Hefei, People's Republic of China

*These authors contributed equally to this work

Correspondence: Yongxiang Li, Email liyongxiangamu@163.com

Introduction: The progression of UC to CACRC involves substantial molecular and cellular alterations. A deeper understanding of these changes is essential for identifying potential therapeutic targets and improving disease outcomes.

Methods: We performed scRNA-seq on tissue samples from a patient with coexisting UC and CACRC lesions, including normal colon, UC-affected tissue, and CACRC. Cell clustering, differential gene expression, and KEGG pathway enrichment analyses were conducted to characterize cellular heterogeneity and pathway dynamics.

Results: Thirteen distinct cell clusters were identified, reflecting significant heterogeneity across disease stages. Six major cell types—B cells, T cells, epithelial cells, monocytes, neutrophils, and CMPs—were selected for in-depth analysis. Epithelial cells from UC samples showed marked upregulation of inflammatory genes such as IL-17A, CXCL1, IL-6, MMP3, and TNFAIP3, which were downregulated in CACRC. KEGG analysis revealed IL-17 signaling as a key pathway involved in disease progression. A progressive increase in Tregs, supported by elevated CD25 expression, was observed from normal tissue through UC to CACRC. Furthermore, C-MYC was significantly upregulated in CACRC epithelial cells, suggesting its role in tumor proliferation and metabolic reprogramming.

Conclusion: This study uncovers dynamic cellular and molecular changes during the transition from UC to CACRC, highlighting IL-17 signaling, Treg expansion, and C-MYC activation as potential drivers of malignancy and targets for future therapeutic intervention.

Keywords: ulcerative colitis, colorectal cancer, single-cell RNA sequencing, IL-17 signaling pathway, treg cells, epithelial cells

Introduction

Ulcerative colitis (UC) is a chronic, relapsing inflammatory bowel disease (IBD) that primarily affects the colon and rectum.¹ Characterized by persistent inflammation and ulceration of the mucosal lining, UC can significantly impact a patient's quality of life and lead to life-threatening complications.² One of the most serious long-term complications of UC is an increased risk of developing colitis-associated colorectal cancer (CACRC).³ Studies indicate that patients with long-standing UC have a significantly higher risk of CACRC compared to the general population, particularly those with more extensive colonic involvement or persistent inflammation.^{3,4} The transition from chronic inflammation in UC to the development of colorectal cancer involves a multi-step process marked by a series of genetic, epigenetic, and environmental changes.⁵ However, the molecular mechanisms underlying this transition remain poorly understood. Understanding the cellular and molecular pathways involved in this progression is crucial for developing effective therapeutic strategies and preventive interventions.^{6,7} A growing body of evidence suggests that chronic inflammation plays a pivotal role in tumorigenesis, contributing to the transformation of

normal epithelial cells into malignant ones.⁸ Inflammatory cytokines, chemokines, and other immune-related molecules are thought to create a microenvironment that promotes tumor initiation, growth, and immune evasion.^{9,10} However, the specific pathways and cellular populations driving the progression from UC to CACRC require further investigation to fully elucidate the mechanisms involved. Recent advances in single-cell RNA sequencing (scRNA-seq) technology have provided new opportunities to explore the cellular heterogeneity and molecular signatures underlying disease progression at an unprecedented resolution.¹¹ Unlike bulk RNA sequencing, which averages gene expression across all cells, scRNA-seq allows for the analysis of individual cells, enabling researchers to map distinct cell types and states, identify rare cell populations, and track dynamic changes in cellular composition during disease progression.^{12,13} This approach is particularly well-suited for studying complex diseases like UC and CACRC, where the interplay between immune cells, epithelial cells, and other stromal components is critical in shaping the disease microenvironment.¹⁴ The tumor immune microenvironment plays a central role in the progression from chronic inflammation to malignancy in CACRC. Beyond inflammatory cytokines and chemokines, recent studies have highlighted the dynamic crosstalk between epithelial cells, immune cells, and stromal components that shapes the local immune landscape. In the context of UC, sustained immune activation initially drives recruitment of innate and adaptive immune cells, including macrophages, neutrophils, T cells, and plasma B cells.^{15,16} However, as inflammation persists, a shift toward immunosuppressive phenotypes—such as regulatory T cells (Tregs), myeloid-derived suppressor cells (MDSCs), and tumor-associated macrophages (TAMs)—contributes to immune escape and tumor initiation.^{17,18} Moreover, changes in antigen presentation, cytokine signaling, and immune checkpoint expression further enable tumor cells to evade surveillance.^{19,20} Single-cell and spatial transcriptomic analyses have recently begun to map these TIME alterations in CACRC at high resolution, revealing complex spatial heterogeneity and functional specialization.²¹ A comprehensive understanding of TIME remodeling during the UC-to-CACRC transition is therefore essential for identifying novel immunotherapeutic targets.

In this study, we applied scRNA-seq to analyze tissue samples from a unique clinical case of a patient who simultaneously presented with UC and colorectal cancer. This allowed us to directly compare normal colon tissue, UC lesions, and CACRC lesions within the same patient, providing a comprehensive view of the cellular and molecular changes associated with the progression of UC to CACRC. By characterizing the cellular composition and gene expression profiles in these different tissue states, we aimed to identify key cell populations and molecular pathways involved in this transition. Our scRNA-seq analysis revealed 13 distinct cell clusters across normal, UC, and CACRC tissues, underscoring the cellular heterogeneity within the diseased tissue microenvironment. Among these, we focused on six major cell types—B cells, T cells, epithelial cells, monocytes, neutrophils, and common myeloid progenitors (CMPs)—as these were identified as key players in the progression from inflammation to cancer. Differential gene expression analysis highlighted dynamic shifts in gene expression within these cell populations, reflecting their evolving roles during disease progression.

Notably, our pathway enrichment analysis using KEGG identified the IL-17 signaling pathway as a central player in the progression from UC to CACRC. This pathway, known for its role in promoting inflammation, has been implicated in various cancers, including CACRC. In this study, we validated the involvement of IL-17-related molecules—such as IL-17A, CXCL1, IL-6, MMP3, and TNFAIP3—using PCR, showing that these genes were upregulated in UC tissues but significantly downregulated in CACRC, suggesting a shift in the inflammatory landscape during disease progression. Furthermore, the increased presence of Tregs, as indicated by elevated CD25 expression, was observed in both UC and CACRC tissues, highlighting their role in modulating immune responses and contributing to tumorigenesis. Additionally, the upregulation of C-MYC in CACRC points to its involvement in tumor cell proliferation and metabolic reprogramming, reinforcing its role as a potential therapeutic target. By integrating scRNA-seq data with pathway analysis and gene expression validation, this study provides new insights into the cellular and molecular mechanisms driving the progression from UC to CACRC. Our findings suggest that the interplay between inflammatory pathways, immune cell dynamics, and epithelial cell proliferation is critical in this transition, offering potential targets for early intervention and therapy.

Methods

Materials

Chromium Single Cell 3' Library & Single Cell 3' v3 Gel Beads (Chromium, PN-1000075); Qubit dsDNA Assay Kit (Life Technologies, Q328520); Qubit dsDNA Assay Kit (Life Technologies, Q328520); DynaBeads[®] MyOne[™] Silane

Beads (Life Technologies, 37002D); Agilent High Sensitivity DNA Kit (Agilent, 5067–4626); SPRIselect Reagent Kit (Life Technologies, B23318); Buffer EB (19086).

Sample Collection

Colon tissue samples, including normal colon tissue, ulcerative colitis-affected tissue, and colorectal cancer tissue, were obtained from the same individual undergoing surgical resection. The tissues were immediately preserved in tissue preservation solution to ensure the preservation of cellular integrity and RNA quality.

Tissue Dissociation

Tissue samples were finely chopped and enzymatically dissociated using a mixture of collagenase, DNase I, and hyaluronidase. The resulting cell suspension was then passed through a 70 μm cell strainer to eliminate debris and isolate single cells.

GEM Generation & Barcoding

Using the 10x Genomics Chromium system, single cells were encapsulated into nanoliter-scale Gel Bead-in-Emulsions (GEMs). Each GEM contained reagents for cell lysis and reverse transcription, as well as a barcoded gel bead. Following cell lysis, poly-adenylated RNA transcripts were captured by barcoded oligonucleotides on the gel beads, which attached unique molecular identifiers (UMIs) to each transcript. This process allows for the unique identification of cDNA generated from each cell, ensuring precise downstream analysis.

Post GEM–RT Cleanup & cDNA Amplification

Following reverse transcription (RT) within the GEMs, the emulsions were disrupted to retrieve the barcoded cDNA. The cDNA was then purified to eliminate excess reagents, primers, and contaminants. This was followed by PCR amplification to produce sufficient cDNA quantities for subsequent library preparation and sequencing. This amplification step is crucial for ensuring comprehensive and accurate representation of each single cell's transcriptome in downstream analyses.

3' Gene Expression Library Construction

To construct the 3' gene expression libraries, the amplified cDNA was first fragmented and then size-selected for optimal length. The cDNA fragments underwent end repair, A-tailing, and adapter ligation. Post-ligation, the adapter-ligated cDNA fragments were enriched through PCR to produce the final library. This preparation ensures that the 3' ends of transcripts are captured, allowing for accurate quantification of gene expression levels in each single cell.

Sequencing

The prepared libraries were sequenced on an Illumina NovaSeq 6000 platform to achieve a depth sufficient to capture the transcriptome of individual cells. Sequencing reads were then processed to filter out low-quality reads and aligned to the reference human genome (GRCh38) using the Cell Ranger pipeline.

Post Library Construction QC

Following library construction, quality control (QC) was conducted to verify the libraries' integrity and readiness for sequencing. Concentration, fragment size distribution, and purity were evaluated using the Agilent Bioanalyzer, Qubit fluorometry, and quantitative PCR (qPCR). Libraries that met the quality criteria were pooled in equimolar ratios for sequencing, ensuring precise and dependable downstream analysis.

Real-Time Quantitative Real-Time PCR

Total RNA was extracted from the tissues using TRIzol (Invitrogen, CA, USA) following the manufacturer's protocol. Reverse transcription of equal amounts of total RNA was performed using an RT-PCR reaction kit (11141ES60, Yeasen Biotechnology, Shanghai, China). Quantitative real-time PCR was performed using qPCR SYBR Green Master Mix (11202ES03, Yeasen Biotechnology, Shanghai, China). All experiments were independently replicated three times. The

expression levels were normalized to GAPDH (General Biotech, Anhui, China) and analyzed using the $2^{-\Delta\Delta Ct}$ method. All primers were synthesized by General Biotech (Anhui, China) and the sequences of primers are listed in Table 1.

Immunofluorescence (IF) Staining

For IF staining of tissue samples, paraffin sections were first deparaffinized with xylene and rehydrated through a graded ethanol series, followed by antigen retrieval in 0.01 M sodium citrate buffer (pH 6.0) for 10–20 minutes. Frozen or unfixed tissues were fixed with 4% paraformaldehyde for 15 minutes. After washing with PBS, samples were permeabilized with 0.1% Triton X-100 (X100, SigmaAldrich) for 10 minutes, and nonspecific binding was blocked by incubating in 5% BSA (SRE0098, SigmaAldrich) for 1 hour at room temperature. Primary antibodies (CD25, abcam, ab231441; C-MYC, abcam, ab32072; IL-17, abcam, ab175380) were applied and incubated overnight at 4°C, followed by incubation with fluorescently labeled secondary antibodies for 1 hour in the dark. DAPI (BL739A, Biosharp, Shanghai, China)-containing mounting medium was used for nuclear staining and coverslipping. The samples were visualized using a fluorescence microscope with appropriate filters. Image J was used to quantify the degree of fluorescence.

Statistical Analysis

All statistical analyses were performed using R or Python. P-values were adjusted for multiple testing using the Benjamini-Hochberg method, and results with adjusted p-values < 0.05 were considered statistically significant.

Results

scRNA-Seq and Cell Typing of Colon Tissues

In clinical practice, we identified a case of ulcerative colitis progressing to colorectal cancer. In the colectomy specimen from this patient, both ulcerative colitis lesions and colorectal cancer lesions were present simultaneously (Figure 1A). Histopathological examination using H&E staining confirmed this finding in tissue samples collected from different affected areas (Figure 1B). Subsequently, we performed single-cell RNA sequencing on three groups of tissue samples to investigate the molecular mechanisms underlying the progression from ulcerative colitis to colorectal cancer. The workflow for single-cell sequencing is illustrated in Figure 1C. Once normal, UC and CAC tissues were obtained, it was rapidly digested to a single-cell suspension and analyzed using scRNA-seq involving a single-tube protocol with unique transcript counting through barcoding with UMIs. After sequencing, we performed additional quality control on the experimental data based on the initial quality control by Cell Ranger. This process involved removing data from multiplets, doublets, or cells with poor capture, followed by downstream analysis. The violin plots in Figure 1D display the distribution of key quality metrics after filtering, including the number of genes per cell (nGene), the number of UMIs per cell (nUMI), the ratio of genes per UMI ($\log_{10} \text{GenesPerUMI}$), the percentage of mitochondrial UMIs (percent_mito), and the percentage of hemoglobin genes (percent_HB). Through the analysis of single-cell sequencing data, we identified 13 distinct cell clusters, with the number of cells in each cluster clearly defined and marked by different colors (Figure 1E). These clusters represent the cellular heterogeneity within the sample, reflecting the distribution of different cell subpopulations or states within the tissue. Further characterization of these clusters allows us to identify various cell

Table 1 The forward and reverse primer sequences (5' → 3') used for the amplification of target genes including GAPDH, IL17A, CXCL1, IL-6, MMP3, and TNFAIP3 in quantitative RT-qPCR assays.

Primer	Forward Primer Sequence (5' → 3')	Reverse Primer Sequence (5' → 3')
GAPDH	GGAGCGAGATCCCTCCAAAAT	GGAGCGAGATCCCTCCAAAAT
IL17A	TCCCACGAAATCCAGGATGC	GGATGTTGAGTTGACCATCAC
CXCL1	ATAAAGGGAGCTGAGAGTGG	CTTCAGGAACAGCCACCACT
IL-6	ACTCACCTCTTCAGAACGAATTG	CCATCTTTGGAAGGTTGAGGTTG
MMP3	AGTCTTCCAATCCTACTGTTGCT	TCCCCGTCACCTCCAATCC
TNFAIP3	TCCTCAGGCTTTGTATTGAGC	TGTGTATCGGTGCATGGTTTAA

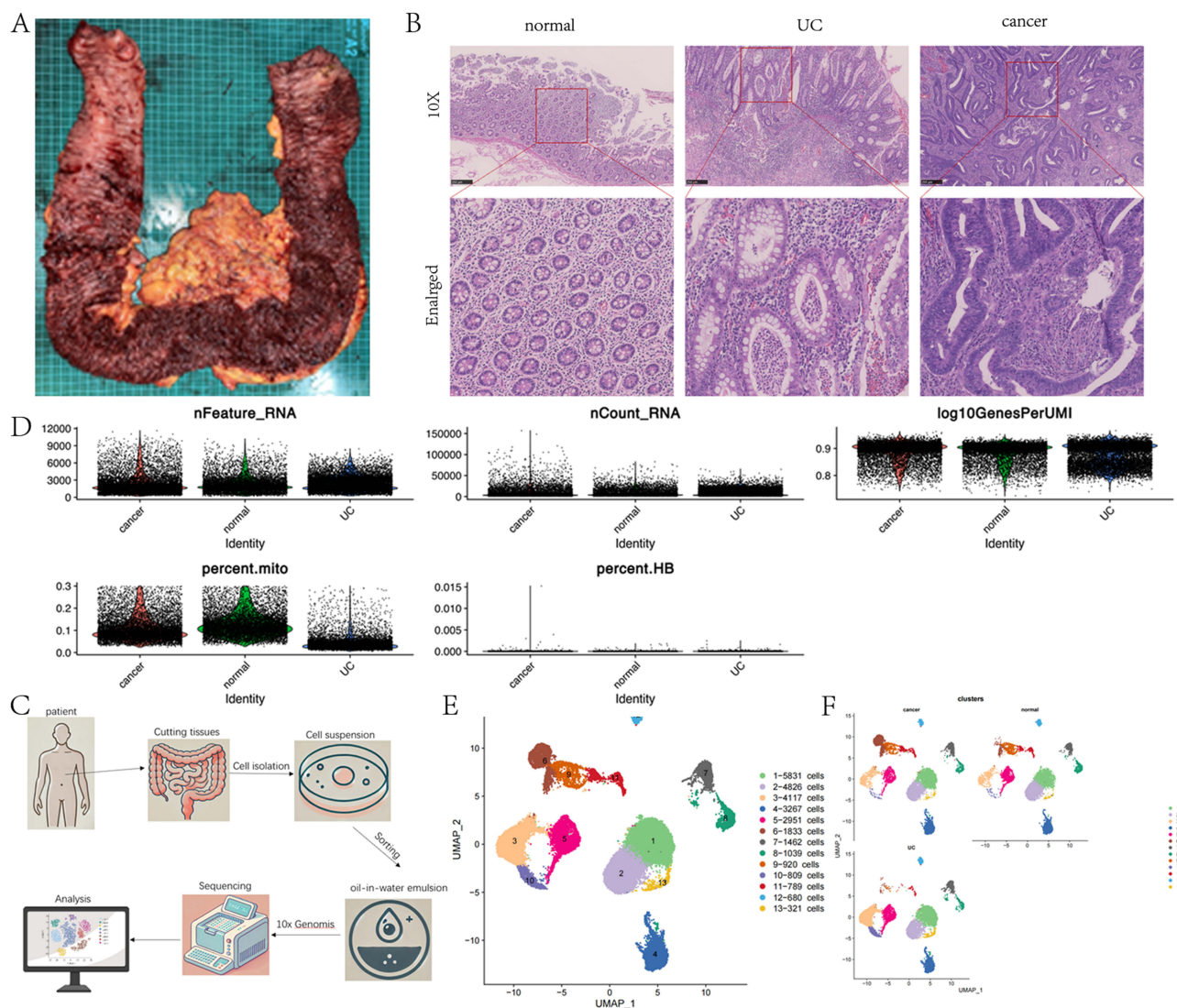


Figure 1 Multimodal analysis of tissue samples. **(A)** Gross image of a colon resection specimen showing areas of ulcerative colitis and adjacent colorectal cancer. **(B)** H&E staining of tissue sections from normal, UC, and CACRC samples at 10X magnification and their respective enlarged views, showing normal epithelial structure, inflamed and dysplastic regions in UC, and invasive dysplasia in CACRC. **(C)** Workflow of the single-cell RNA sequencing process: Tissue is isolated from the patient, cells are dissociated into a suspension, sequenced using 10x Genomics, and analyzed for gene expression profiles. **(D)** Quality control metrics of the single-cell RNA-seq data: nFeature_RNA, nCount_RNA, log10GenesPerUMI, percent.mito (mitochondrial content), and percent.HB (hemoglobin content) across normal, UC, and cancerous tissues. **(E)** UMAP plot showing clustering of cells based on transcriptional profiles from normal, UC, and CACRC tissues, with color-coded identities, labeled by cell types. **(F)** UMAP plot displaying individual clusters, labeled by cell types, in normal, UC, and cancer tissues, highlighting distinct cellular populations and their distribution across the disease stages.

types or subpopulations with distinct functional states. Next, we displayed the identified cell clusters by grouping them into three categories: normal tissue, ulcerative colitis tissue, and colorectal cancer tissue (Figure 1F). This result highlights the distribution patterns of cell populations across different tissue states. By organizing the clusters according to their tissue of origin, we can more clearly observe the differences in cell composition between normal, ulcerative colitis, and colorectal cancer tissues. This distribution pattern reveals the potential dynamic changes in specific cell subpopulations during the progression from normal tissue to pathological conditions.

Identification of Key Cell Types and Pathways Involved in the Progression from Ulcerative Colitis to Colorectal Cancer

We performed preliminary annotation of the cell clusters, with each color representing a specific cell type (Figure 2A). This result provides an initial overview of the distribution of different cell types across normal, ulcerative colitis, and

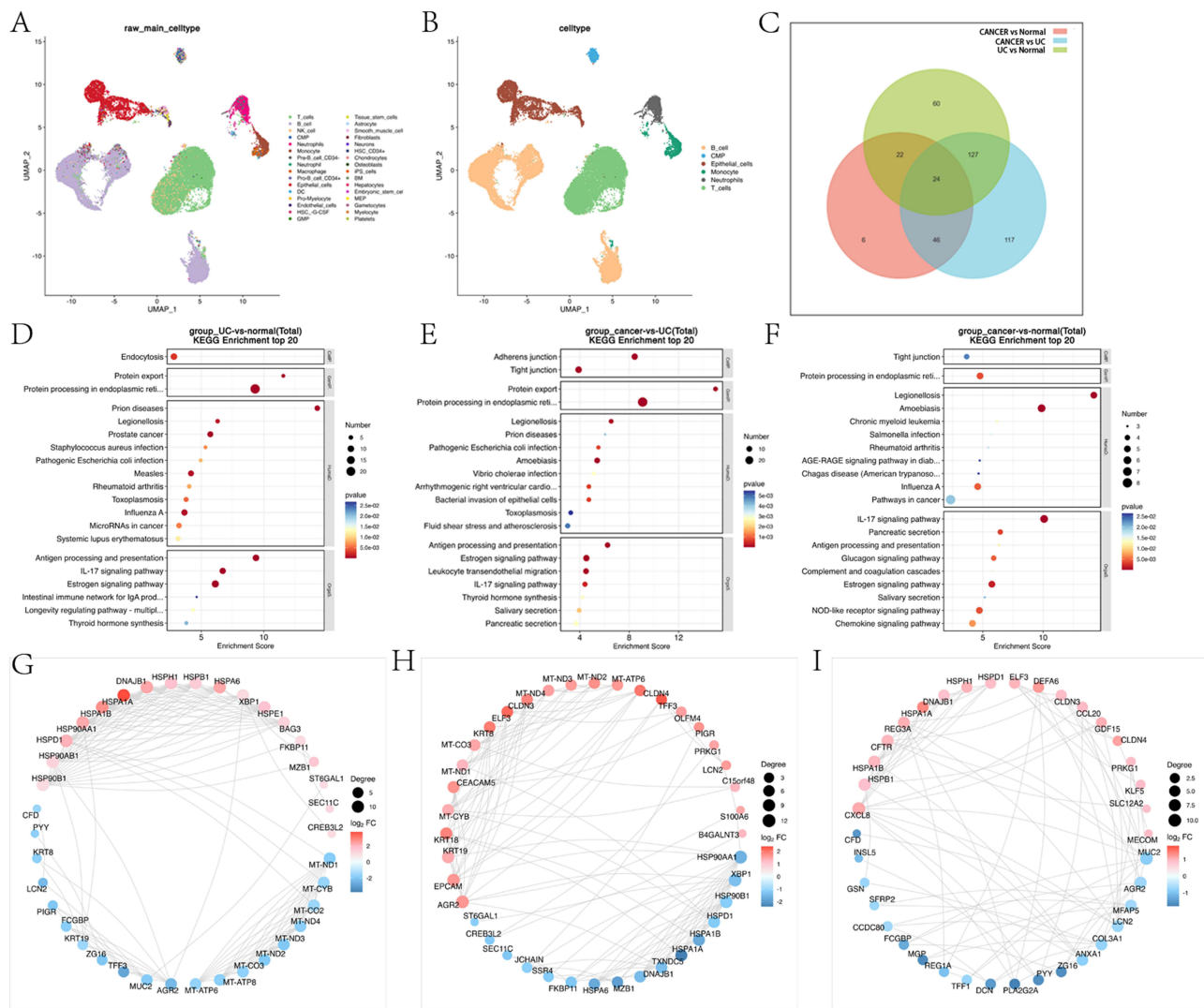


Figure 2 Single-cell RNA sequencing analysis and pathway enrichment. **(A and B)** UMAP plots showing the distribution of major cell types in normal, UC, and CACRC tissues, before **(A)** and after **(B)** cell type identification. Different cell populations are color-coded, including B cells, T cells, epithelial cells, and other immune or stromal cell types. **(C)** Venn diagram illustrating the overlap of differentially expressed genes (DEGs) across three comparisons: cancer vs normal, cancer vs UC, and UC vs normal. Shared and unique gene sets are displayed in the intersections of the diagram. **(D–F)** KEGG pathway enrichment analysis for DEGs across disease stages. **(D)** UC vs normal, **(E)** cancer vs UC, and **(F)** cancer vs normal. Top 20 pathways are shown, with enrichment scores and p-values indicated by dot size and color. Key pathways include IL-17 signaling, protein processing, and antigen presentation. **(G–I)** Protein-protein interaction (PPI) networks derived from DEGs for **(G)** UC vs normal, **(H)** cancer vs UC, and **(I)** cancer vs normal comparisons. Nodes represent individual proteins, with color gradients indicating fold change (log2FC), and edges represent interactions between proteins. Key proteins and pathways are highlighted, emphasizing their roles in disease progression.

colorectal cancer tissues. To further investigate the impact of different cell types on disease progression, we selected the top six cell types based on their relative proportions: B cells, T cells, epithelial cells, monocytes, neutrophils, and CMP (Figure 2B). The selection of these major cell types allows us to focus on the key cell populations that play a critical role in disease onset and progression, providing insights into their dynamic changes and potential biological functions across normal, ulcerative colitis, and colorectal cancer tissues. By performing pairwise comparisons of differentially expressed genes between the ulcerative colitis group and the normal group, the colorectal cancer group and the normal group, and the ulcerative colitis group and the colorectal cancer group, we identified the differential genes between each pair of sample groups. To further investigate the changes in genes during disease progression, we constructed Venn diagrams of these differential genes (Figure 2C) to identify genes that play important roles throughout the progression. Next, we conducted a KEGG pathway analysis of the differentially expressed protein-coding genes and calculated the significance of gene enrichment in each pathway using a hypergeometric test. Figures 2D–F display the KEGG enrichment details

between the normal group, ulcerative colitis group, and colorectal cancer group, revealing that the IL-17 signaling pathway plays a critical role in the progression of intestinal tissue from normal to ulcerative colitis and then to colorectal cancer. Finally, we created circular interaction plots of the top 25 upregulated and downregulated differentially expressed genes in the three sample groups (Figures 2G–I) to visually represent the complex relationships between these genes and further explore their potential biological functions.

Heterogeneity, Differentiation Trajectories, and Functional Roles of B Cell Subtypes in Disease Progression and Drug Sensitivity

Figure 3A shows the clustering distribution of cell populations. Through UMAP dimensionality reduction analysis, cells in the sample are divided into several distinct clusters, which represent different types of B cells and their associated cells. The presence of multiple clusters reflects the heterogeneity and complexity of the cells in the sample, suggesting the potential existence of multiple functional B cell subtypes. Figure 3B further divides B cells into multiple subtypes, each of which shows a distinct distribution pattern on the UMAP plot. Cycling plasma B cells cluster in a specific region,

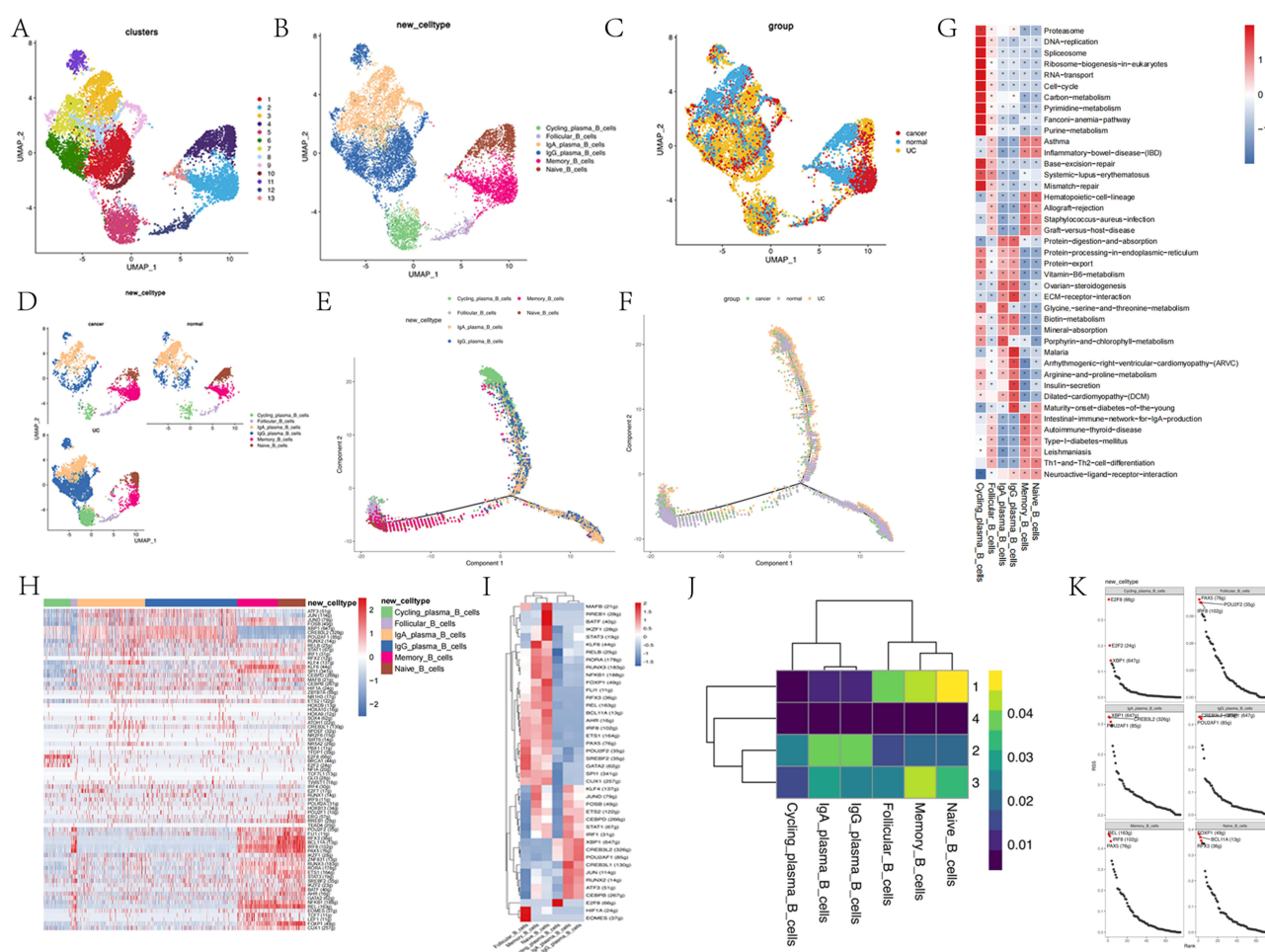


Figure 3 Single-cell transcriptomic analysis of B cell subpopulations. (A–C) UMAP plots showing clustering of B cell subpopulations from normal, UC, and CACRC samples. (A) Clusters are color-coded by cell groups. (B) Cell type identification reveals distinct subpopulations, including cycling plasma B cells, follicular B cells, memory B cells, and naive B cells. (C) The same UMAP plot, color-coded by disease state: normal, UC, and CACRC. (D) Separate UMAP plots displaying the distribution of B cell subpopulations in normal, UC, and CACRC tissues. (E) Pseudotime trajectory analysis showing the developmental progression of B cells across disease states. (F) Pseudotime heatmap demonstrating changes in gene expression across the trajectory of B cell differentiation from naive to cycling plasma B cells. (G) Pathway enrichment analysis for differentially expressed genes in B cell subtypes, highlighting significant pathways such as antigen presentation, ribosome biogenesis, and oxidative phosphorylation, with color intensity representing fold enrichment. (H) Heatmap showing the expression of top differentially expressed genes across B cell subtypes. (I) Clustered heatmap comparing gene expression patterns between B cell subtypes in normal, UC, and CACRC tissues. (J) Hierarchical clustering analysis of the identified B cell subpopulations, showing relationships between different subtypes based on gene expression profiles. (K) GSEA plots for selected hallmark pathways, including oxidative phosphorylation, MYC targets, and inflammatory response pathways, with significant enrichment in different B cell populations.

while other subtypes, such as Memory B cells, form relatively separated clusters in different regions, indicating functional and differentiation differences among the subtypes. **Figure 3C** illustrates the distribution pattern of B cells under different disease conditions. Cells from the normal group are relatively concentrated on the UMAP plot, while cells from the cancer and UC groups are dispersed across multiple regions. Notably, certain cell subtypes in the cancer group exhibit significant spatial expansion, suggesting that disease conditions influence B cell distribution and differentiation. **Figure 3D** visualizes the distribution of B cell subtypes across normal, UC, and cancer states. The expansion of certain subtypes is especially evident in the cancer state, with an increased proportion of Cycling plasma B cells observed in both cancer and UC, indicating that these subtypes may be associated with disease progression. **Figure 3E** shows the differentiation trajectory of B cell subtypes, revealing the developmental pathway of B cells from an initial state (Naive B cells) to a mature state (such as Memory B cells). This analysis suggests that Cycling plasma B cells may represent an intermediate state between naive and mature B cells. **Figure 3F** further reveals the differentiation trajectory of B cells under different disease states. Compared to normal cells, B cells in cancer and UC display significant trajectory expansion, particularly in the differentiation process of Cycling plasma B cells, where cells from cancer and UC states deviate along specific paths, suggesting that these cells may have unique differentiation characteristics under these conditions. **Figure 3G** reveals the involvement of various B cell subtypes in key signaling pathways. For example, Cycling plasma B cells show significant enrichment in pathways related to DNA replication and ribosome biogenesis, while Memory B cells are more active in immune-regulatory pathways. These pathway differences may be associated with functional changes in B cells under different disease conditions. **Figure 3H** presents the gene expression heatmap of B cell subtypes, showing the specific gene expression patterns of each subtype. For example, genes related to cell proliferation are significantly upregulated in Cycling plasma B cells, while Memory B cells exhibit upregulation of genes associated with immune memory. This gene expression difference reveals the potential functions of each subtype in immune responses. **Figure 3I**, through pathway enrichment analysis, shows the involvement of different B cell subtypes in critical biological pathways. Cycling plasma B cells display upregulation of cell cycle-related pathways, while Naive B cells show some activity in metabolism-related pathways, suggesting functional differences among these subtypes during disease progression. **Figure 3J** displays a quantitative heatmap of B cell subtype distributions across distinct sample clusters, further confirming compositional differences and the enrichment of certain B cell subsets, such as Cycling plasma B cells and Naive B cells, in specific conditions. **Figure 3K** illustrates the drug sensitivity analysis of different B cell subtypes. Cycling plasma B cells exhibit higher sensitivity to certain drugs, suggesting that this subtype may be a potential therapeutic target for these drugs. Through UMAP dimensionality reduction, pseudotime differentiation trajectory analysis, and functional pathway enrichment analysis, the study reveals the distribution, differentiation, and functional differences of various B cell subtypes in normal, ulcerative colitis, and cancer states. Cycling plasma B cells show significant expansion under disease conditions and are actively involved in pathways related to cell proliferation and immune regulation. Additionally, they exhibit high sensitivity to specific drugs, suggesting their potential role as key players in disease progression and as promising therapeutic targets.

Heterogeneity and Progression of T Cell Subtypes and Immune Responses from Normal Tissue to Ulcerative Colitis and Colorectal Cancer

Figure 4A illustrates the distribution of T cells at the single-cell level using UMAP for dimensionality reduction according to groups. In **Figure 4B**, a more refined analysis classifies T cells into several subtypes. Each subtype represents T cells in different functional states, such as cytotoxic-CD8 T cells, exhausted-CD4/CD8 T cells, memory-CD8 T cells and regulatory T cells (Treg). The differences between these subtypes may reflect the distinct roles of T cells in normal tissue, ulcerative colitis (UC) tissue, and colorectal cancer tissue, suggesting the heterogeneity of T cell immune responses across these disease states. In **Figure 4C** and **D**, we present the UMAP of T cell subtypes stratified by sample groups, revealing distinct proportions of T cell subtypes across the three tissue types. Notably, the proportion of Treg cells increases progressively from normal tissue, through ulcerative colitis (UC) tissue, to colorectal cancer tissue. The increasing proportion of naive CD4⁺ T cells may reflect either an impaired differentiation process or an influx of less differentiated T cells in response to chronic inflammation and tumorigenesis. **Figure 4E** illustrates the clustering

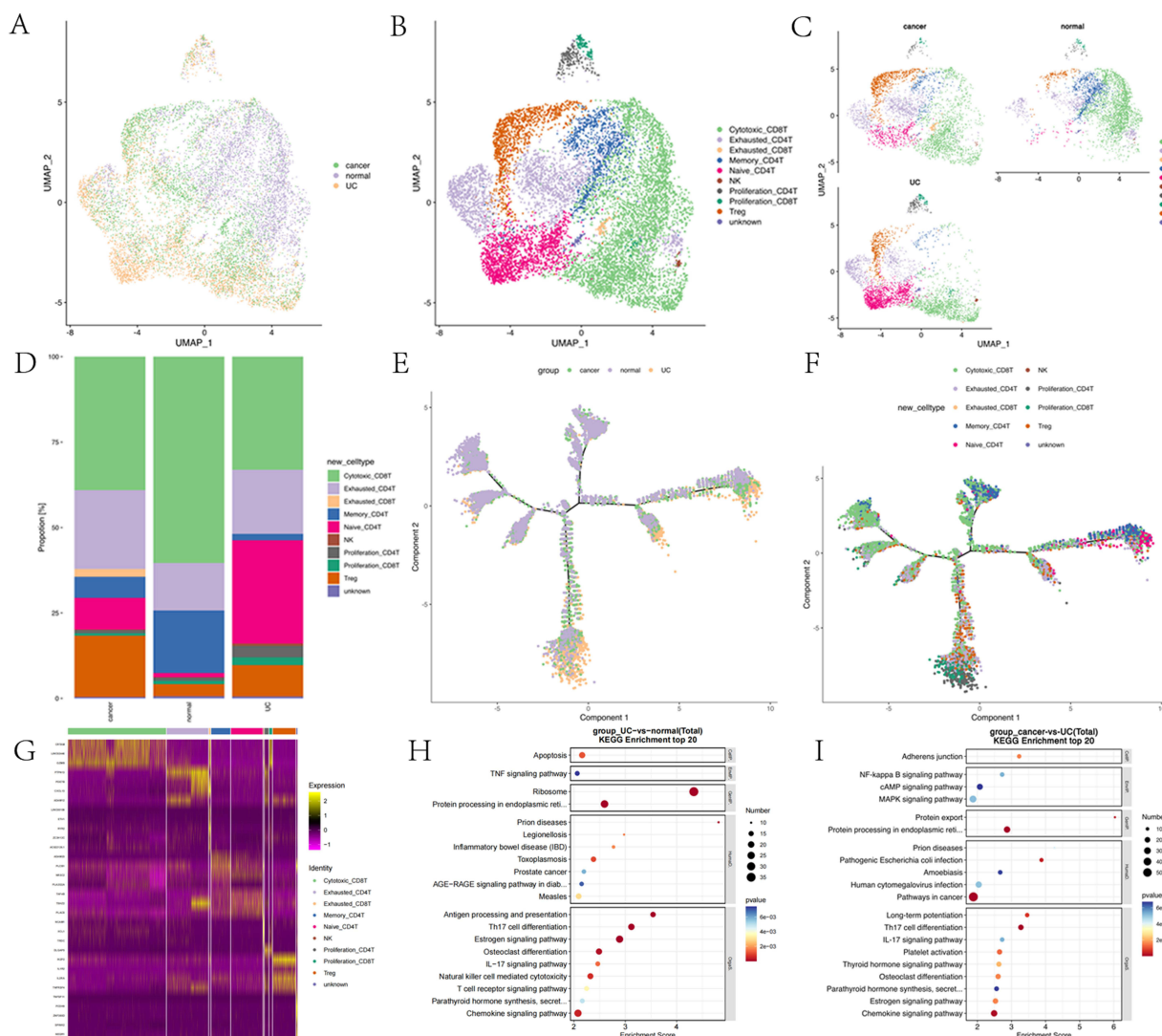


Figure 4 Single-cell RNA-seq analysis of CD8+ T cell subpopulations. (A–C) UMAP plots displaying CD8+ T cell subtypes across normal, UC, and CACRC samples. (A) Cells are color-coded by disease state (normal, UC, CACRC). (B) Major CD8+ T cell subtypes, including cytotoxic CD8+ T cells, exhausted CD8+ T cells, memory CD8+ T cells, proliferating CD8+ T cells, Tregs, and NK cells, are identified and color-coded. (C) Separate UMAP plots show the distribution of CD8+ T cell subtypes within cancer, normal, and UC tissues. (D) Stacked bar plot representing the proportions of CD8+ T cell subtypes in normal, UC, and CACRC tissues. (E and F) Pseudotime trajectory analysis showing the differentiation path of CD8+ T cells across normal, UC, and CACRC tissues. (E) Cells are colored by disease state, and (F) cells are colored by identified CD8+ T cell subtype, highlighting changes along the developmental trajectory. (G) Heatmap displaying the expression of top differentially expressed genes (DEGs) across identified CD8+ T cell subtypes in normal, UC, and CACRC tissues. (H and I) KEGG pathway enrichment analysis of DEGs. (H) UC vs normal and (I) CACRC vs UC. Pathways such as TNF signaling, IL-17 signaling, NF-kappa B signaling, and apoptosis are significantly enriched, with dot sizes representing the number of DEGs and color intensity indicating p-values.

distribution of cells from three different sample groups, depicting their relationships in a low-dimensional space. Different colors represent the respective sample groups: normal group (purple), cancer group (green), and UC group (orange). Cells from the normal group are distributed more widely, covering multiple branches of the plot, while cells from the cancer and UC groups are more concentrated in specific branches. Specifically, different T cell subpopulations are clustered in various branches of the plot to varying extents (Figure 4F). Cytotoxic CD8+ T cells (green) are distributed across multiple branches, indicating their broad involvement in the overall immune response. Memory CD4+ T cells (pink) and naive CD4+ T cells (red) are mainly concentrated in distinct branches, suggesting their divergent roles in immune function. Exhausted T cells in ulcerative colitis are clustered in certain branches, indicating impaired or exhausted T cell function during the progression of the disease. Figure 4G reveals significant changes in gene expression profiles among different T cell subpopulations during the progression from normal tissue to ulcerative colitis

(UC) and eventually to cancer. Cytotoxic CD8⁺ T cells and exhausted T cells exhibit differential expression of specific genes throughout disease progression, indicating their distinct roles and states in immune responses. The upregulation of genes such as CXCL13 and TNFRSF4 in UC and cancer suggests that these genes may play critical roles in immune suppression, inflammatory responses, and T cell exhaustion. Overall, the figure highlights the complexity of T cell-mediated immune regulation and suggests potential molecular mechanisms underlying the transition from UC to cancer. **Figure 4H** and **I** illustrate the progressive intensification of immune and inflammatory responses in T cells, as well as the activation of cancer-related signaling pathways, during the transition from normal tissue to ulcerative colitis (UC) and eventually to colorectal cancer. In UC, the significant enrichment of the IL-17 signaling pathway and Th17 cell differentiation suggests that inflammatory responses play a central role in UC pathogenesis. As the disease progresses to cancer, cancer-related pathways, such as MAPK and NF-kappa B, are notably activated, indicating their potential involvement in promoting cell proliferation and immune evasion during tumor development. These findings suggest that inflammation-driven immune dysregulation, along with the activation of cancer-associated signaling pathways, may underlie the transition from UC to cancer.

The Impact of CNV Levels on Gene Expression, Cell Classification, and Disease Progression

Figure 5A shows a UMAP projection of cells categorized by their CNV status (CNV_high, CNV_median, CNV_low). This distribution indicates a clear separation between different CNV states, suggesting that CNV alterations may contribute to functional or pathological differences among these cell populations. In **Figure 5B**, several genes, such as CKMT2, LINC01748, and SLC22A3, are significantly upregulated in the CNV_high group. These genes may be associated with cell proliferation, genomic instability, or tumor progression, as cells with high CNV are often linked to more aggressive disease phenotypes, such as cancer. In contrast, the expression of certain genes, such as PRKAA2, RHBOL2, and VSIG2, is markedly reduced in the CNV_low group. These genes may be related to stable cellular functions or normal cell behavior, suggesting that CNV_low cells are more likely to be in a healthy or homeostatic state. By combining the UMAP clustering plot and the group classification plot (**Figure 5C** and **D**), a clear correlation between cell clusters and their respective disease states is observed. Based on UMAP dimensionality reduction analysis, cancer cells are predominantly located in the upper part of the UMAP, while normal cells are primarily distributed in the lower region. Ulcerative colitis (UC) cells exhibit a more dispersed distribution, with some overlapping with cancer cells and others with normal cells. This suggests that UC may represent an intermediate stage in the transition from normal tissue to a cancerous state. Further analysis reveals that clusters 1 and 2 are closely associated with the cancer state, while clusters 3 and 4 are more related to the normal state. The distribution pattern of UC cells indicates that their gene expression may exhibit characteristics of both normal and cancer states. This description effectively highlights the correlation between cell populations and disease states, emphasizing the role of UC as a potential transitional phase in disease progression. **Figure 5E** illustrates the distribution of CNV levels across different disease states. The majority of cancer cells exhibit high CNV levels (green), while normal cells are predominantly distributed in the low and medium CNV levels (orange and purple, respectively). UC cells primarily show low CNV levels, indicating significant differences in CNV levels between cells from different disease states. **Figure 5F** further demonstrates the distribution of cells based on CNV levels. High CNV level cells (green) are primarily concentrated in the cancer region, while low CNV level cells (orange) are clustered in the normal tissue and UC areas. This suggests a strong correlation between CNV levels and the disease state of the cells. **Figure 5G** shows the distribution of different cell clusters along the disease progression. **Figure 5H**, categorized by disease state, illustrates the temporal distribution of cancer, normal tissue, and UC cells along the pseudotime trajectory. Cancer cells are located at the later stage of the pseudotime trajectory, while normal cells are distributed at the early stage, and UC cells are positioned in the middle. This further supports the notion that UC may represent a transitional phase between normal tissue and cancer. **Figure 5I**, a pseudotime trajectory classified by CNV levels, shows that cells with high CNV levels are concentrated at the later stages of the trajectory, indicating their association with more advanced disease states (eg, cancer), while cells with low CNV levels are concentrated at the early stages, likely corresponding to normal tissue. This further highlights the critical role of CNV levels in disease

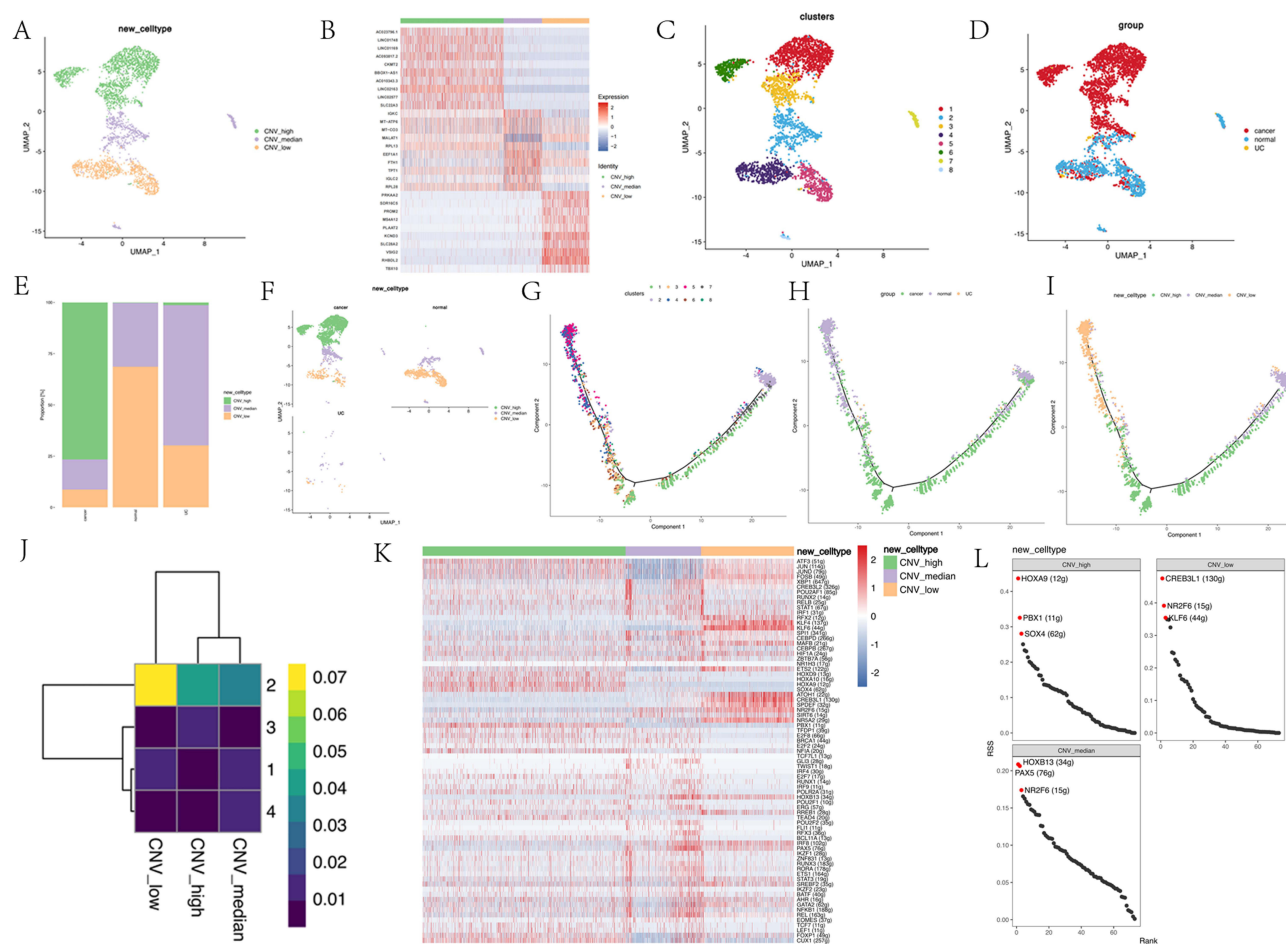


Figure 5 Analysis of CNV in different cell subpopulations from tissues. **(A)** UMAP plot displaying cell subpopulations with different CNV levels: CNV-high, CNV-medium, and CNV-low. **(B)** Heatmap showing the expression of top differentially expressed genes (DEGs) across CNV-high, CNV-medium, and CNV-low subpopulations, with color intensity representing gene expression levels. **(C)** UMAP plot clustering the identified cell populations based on transcriptional profiles, color-coded by cluster identity. **(D)** UMAP plot showing the distribution of cells based on disease state: normal, UC, and CACRC. **(E)** Stacked bar plot depicting the proportions of CNV-high, CNV-medium, and CNV-low subpopulations across normal, UC, and CACRC samples. **(F)** UMAP plot separating CNV-high, CNV-medium, and CNV-low subpopulations in normal, UC, and CACRC tissues. **(G–I)** Pseudotime trajectory analysis illustrating the progression of cells along the developmental axis, colored by **(G)** cluster identity, **(H)** disease group, and **(I)** CNV level (high, medium, low). **(J)** Hierarchical clustering analysis of CNV-high, CNV-medium, and CNV-low subpopulations based on their transcriptional profiles, with color indicating the strength of clustering. **(K)** Heatmap showing gene expression profiles across CNV subtypes, highlighting key genes associated with CNV-high, CNV-medium, and CNV-low populations. **(L)** Gene set enrichment analysis (GSEA) identifying hallmark CNV-related genes, such as HOXA9, SOX4, and PAX5, within CNV-high, CNV-medium, and CNV-low populations.

progression. The heatmap illustrates the clustering patterns of gene expression under different CNV levels. Cells are grouped into four main clusters based on their gene expression profiles (Figure 5J), with CNV-high cells predominantly clustered within high-expressing gene groups, while CNV-low cells exhibit lower gene expression patterns. This suggests that CNV levels significantly impact gene expression, particularly in cancer-related genes. The heatmap further demonstrates the expression of key transcription factors across cells with varying CNV levels (Figure 5K). In CNV-high cells, transcription factors such as HOXA9 and SOX4 show markedly increased expression, whereas in CNV-low cells, CREB3L1 exhibits higher expression. This indicates that these transcription factors may regulate cellular functions in different CNV contexts. The RSS ranking plot (Figure 5L) highlights significant transcription factor genes across different CNV levels. HOXA9 and PBX1 are top-ranked in CNV-high cells, while CREB3L1 and NR2F6 show higher RSS values in CNV-low cells. These transcription factors likely play crucial roles in regulating disease progression under varying CNV conditions.

UMAP-based clustering (Figure SF1) demonstrates the emergence of distinct epithelial subpopulations in UC and CACRC tissues compared to normal controls. Notably, UC epithelial cells exhibit a pronounced inflammatory phenotype, characterized by increased expression of cytokine response genes and proliferation markers, while CACRC epithelial

cells acquire tumor-associated features, including stemness and metabolic reprogramming. KEGG pathway enrichment analysis (Figure SF2) further highlights the IL-17 signaling pathway as one of the most significantly enriched pathways in epithelial cells from UC tissues. This suggests that IL-17 signaling actively drives inflammatory activation, epithelial-mesenchymal transition (EMT), and disruption of barrier function during active colitis. Genes such as IL-17A, CXCL1, IL-6, MMP3, and TNFAIP3 are highly expressed in UC epithelial cells but show a marked reduction in CACRC, indicating that IL-17-mediated inflammation is particularly active during early disease stages.

Cell Interaction Patterns and Information Flow in UC, Cancer, and Normal Tissues

Figure 6A illustrates the number and strength of cell interactions across different disease states. Cell interactions are most frequent in normal tissues, while the interaction strength is highest in cancer tissues, suggesting that cell signaling in the tumor microenvironment is more active, potentially contributing to cancer progression. Figure 6B and C show the differences in cell interactions between UC and normal tissues. B cells exhibit stronger interactions in both states, whereas epithelial cells show weaker interactions, indicating significant differences in the interaction patterns between immune and epithelial cells in UC and normal tissues. Figure 6D and E reveal the differences in cell interactions between cancer and normal tissues. The interaction between B cells and T cells is significantly enhanced in cancer, indicating that

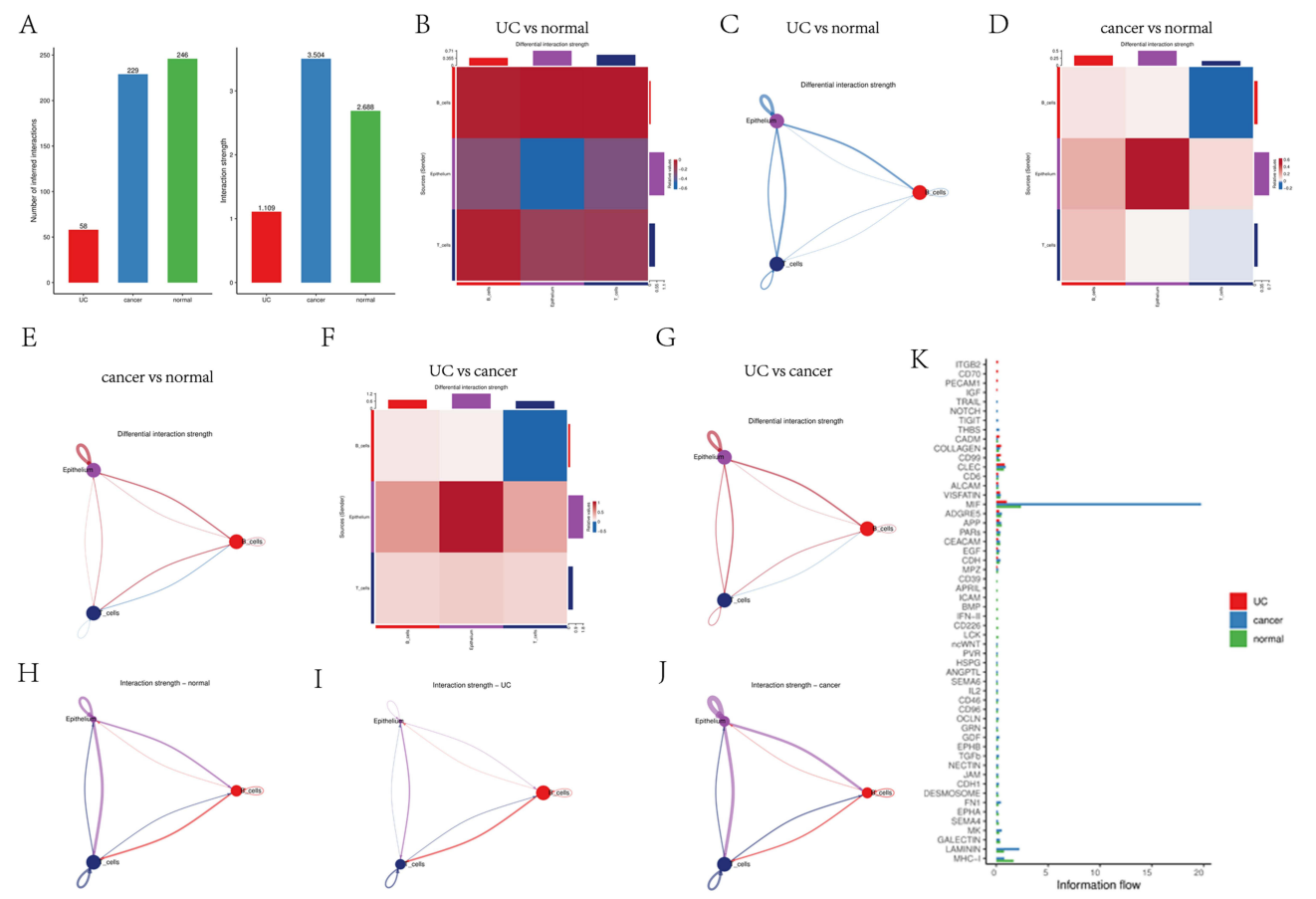


Figure 6 Cell-cell communication and interaction strength analysis in normal, UC, and CACRC tissues. (A) Bar plots showing the number of cell-to-cell interactions and overall interaction strength across UC, CACRC, and normal tissues. UC shows the lowest number of interactions and interaction strength compared to CACRC and normal tissues. (B and C) Heatmap (B) and network plot (C) displaying the differential interaction strength between epithelial cells, immune cells, and stromal cells in UC vs normal tissues. Line thickness in the network plot reflects the interaction strength, with red lines indicating stronger interactions and blue lines indicating weaker ones. (D and E) Heatmap (D) and network plot (E) representing differential interaction strength between cell types in CACRC vs normal tissues. (F and G) Heatmap (F) and network plot (G) showing the interaction differences between UC and CACRC tissues, highlighting changes in the strength of epithelial and immune cell communication. (H-J) Network plots showing the interaction strengths in (H) normal, (I) UC, and (J) CACRC tissues. The thickness of the connecting lines corresponds to the interaction strength, with red indicating stronger and blue indicating weaker interactions. (K) Information flow analysis of ligand-receptor pairs contributing to cell communication across UC, CACRC, and normal tissues. Genes such as ADAM28, CEACAM5, and COL1A1 show significant information flow differences, particularly in CACRC compared to normal and UC tissues.

immune cell interactions in the tumor microenvironment are more frequent, which may be related to immune evasion or tumor proliferation. **Figure 6F** and **G** depict the interaction patterns between UC and cancer tissues. B cell and T cell interactions are significantly enhanced in cancer tissues, while interactions in UC are weaker, further highlighting the distinct communication characteristics of cells in different disease states. **Figure 6H–J** demonstrate the interaction strength in normal, UC, and cancer states. In the cancer state, the interactions between B cells and T cells are the strongest, whereas cell interactions in UC are relatively weaker, indicating more active immune cell communication in the tumor microenvironment. **Figure 6K** shows the information flow across UC, cancer, and normal tissues. The high information flow in B cells and T cells in cancer suggests their critical role in tumor progression, further supporting the active role of immune cells in the cancer microenvironment. This analysis highlights distinct patterns of cell interactions and information flow across UC, cancer, and normal tissues. B cells and T cells demonstrate stronger interactions in cancer tissues, suggesting enhanced immune cell communication in the tumor microenvironment. In contrast, UC tissues exhibit weaker cell interactions, particularly between immune and epithelial cells. The information flow analysis further emphasizes the pivotal role of B cells and T cells in cancer progression, indicating their potential contribution to tumor proliferation and immune evasion. These findings underline the importance of immune cell interactions in shaping disease-specific microenvironments.

Dynamic Expression of Inflammatory and Immune Regulatory Factors During UC and CACRC Progression

Based on the KEGG analysis, which indicated that the IL-17 signaling pathway plays a critical role in the progression of UC and CACRC, we validated the expression of the IL-17 signaling pathway and its downstream related factors in patient tissues using PCR (**Figure 7A–E**). The expression of several key inflammation-related genes (IL-17A, CXCL1, IL-6, MMP3, and TNFAIP3) was significantly upregulated, whereas in colorectal cancer, the expression of these genes was markedly downregulated. These findings suggest that these genes may play critical roles in the inflammatory response of UC, but their functional mechanisms may change during the progression to cancer. Based on the data analysis, we observed an increasing proportion of Treg cells from normal tissue to UC tissue and then to CACRC tissue. To validate this, we used CD25 as a marker and performed immunofluorescence staining. The results showed increased CD25 expression in both UC and CACRC tissues (**Figure 7F** and **I**), suggesting its involvement in inflammatory and tumor immune responses. Subsequently, we validated the expression in epithelial cells, and the results indicated a significant upregulation of C-MYC in CACRC (**Figure 7G** and **I**), highlighting its key role in tumor cell proliferation and metabolic reprogramming. Additionally, we assessed IL-17 expression through immunofluorescence staining. The results demonstrated that high IL-17 expression in UC was associated with enhanced inflammatory responses (**Figure 7H** and **I**), while its reduction in CACRC suggested changes in the role of inflammation during cancer progression. These results indicate that inflammation-related factors such as IL-17A, CXCL1, IL-6, and MMP3 are significantly upregulated during the course of ulcerative colitis, while their expression decreases as the disease progresses to cancer. Immune regulatory factors such as CD25 and TNFAIP3 also exhibit distinct expression patterns in inflammation and tumors. The marked upregulation of C-MYC in cancer suggests that it may be a key molecule in tumor progression.

Discussion

This study provides a detailed exploration of the cellular and molecular dynamics involved in the progression from UC to CACRC using scRNA-seq. Our results revealed distinct shifts in cellular populations and gene expression patterns, shedding light on key mechanisms that contribute to the pathogenesis of CACRC in the context of chronic inflammation. One of the most notable findings was the identification of six key cell types—B cells, T cells, epithelial cells, monocytes, neutrophils, and CMPs—that demonstrated significant changes in abundance and gene expression across normal, UC, and CACRC tissues. These shifts indicate that both immune and non-immune cell populations actively participate in the progression from inflammation to cancer. The expansion of specific cell types, such as Treg cells and cycling plasma B cells, suggests their pivotal roles in modulating the immune environment, potentially facilitating both chronic inflammation in UC and immune evasion in CACRC.

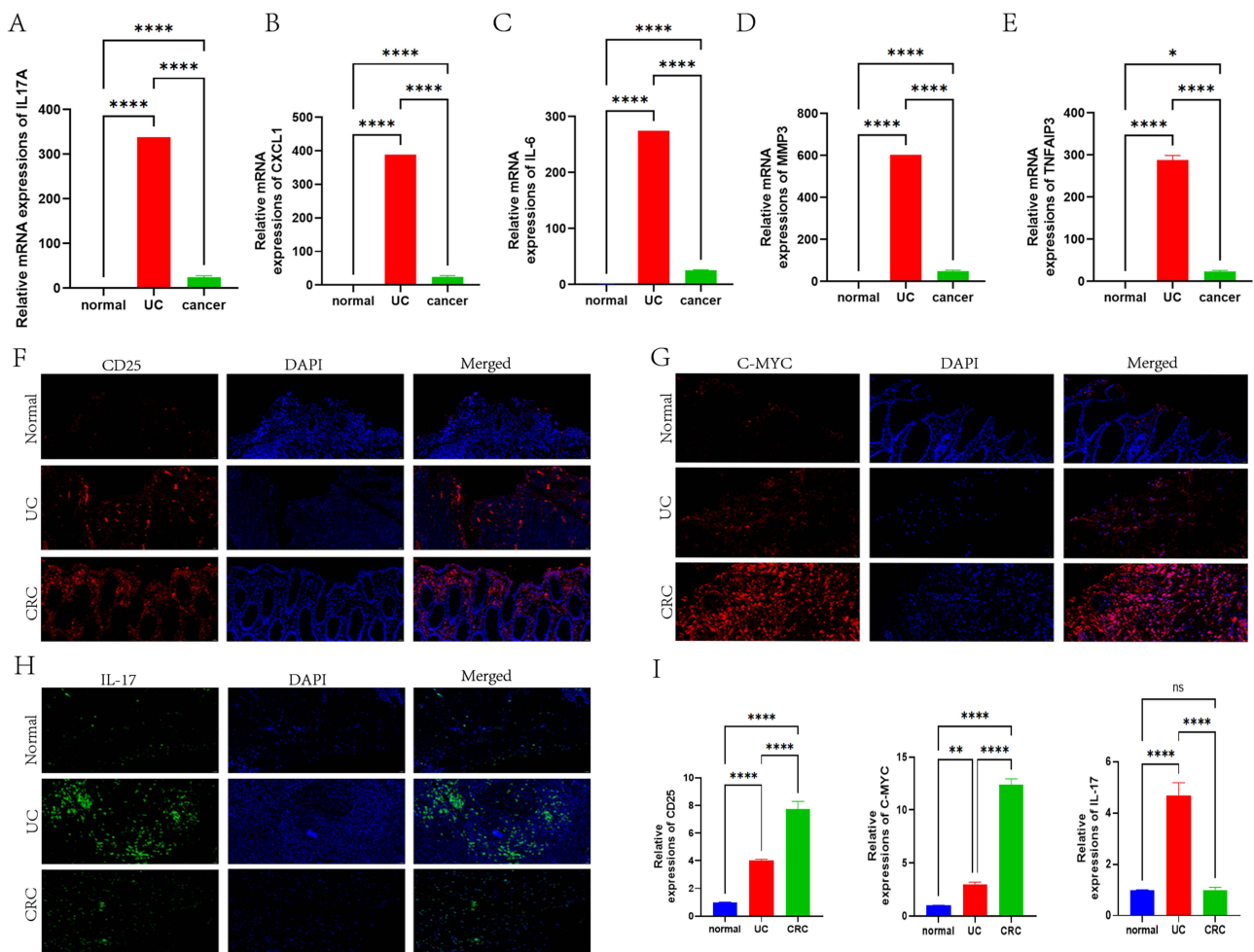


Figure 7 Expression of inflammatory and oncogenic markers in normal, UC, and CACRC tissues. **(A–E)** Quantitative real-time PCR (qPCR) analysis of mRNA levels for pro-inflammatory and oncogenic genes. **(A)** IL-17A, **(B)** CXCL1, **(C)** IL-6, **(D)** MMP3, and **(E)** TNFAIP3 show significantly elevated expression in UC compared to normal and CACRC tissues. Statistical significance is denoted as **** $p < 0.0001$, * $p < 0.05$. **(F–H)** Immunofluorescence staining of **(F)** CD25, **(G)** C-MYC, and **(H)** IL-17 in normal, UC, and CACRC tissues. CD25 and C-MYC show increased expression in CACRC, while IL-17 is elevated in UC tissues. DAPI (blue) is used for nuclear counterstaining. **(I)** Quantification of relative fluorescence intensity for CD25, C-MYC, and IL-17 from immunofluorescence staining in normal, UC, and CACRC tissues. Data show significant increases in CD25 and C-MYC in CACRC, while IL-17 is significantly higher in UC tissues. Statistical significance is denoted as ** $P < 0.01$, **** $p < 0.0001$, ns = not significant.

The observation of increasing Treg cell populations and their elevated expression of CD25 in both UC and CACRC raises critical questions about the balance between immune regulation and immune tolerance during disease progression.²² The dual role of Tregs in controlling excessive inflammation while potentially promoting an immunosuppressive tumor microenvironment highlights the fine line between beneficial and harmful immune modulation.^{23,24} These findings align with previous studies suggesting that Tregs, while crucial for maintaining homeostasis during inflammation, might create a permissive environment for tumor growth by hindering effective anti-tumor immune responses. This makes Tregs a promising target for immunotherapeutic interventions aimed at boosting anti-tumor immunity without exacerbating inflammatory diseases like UC.

The IL-17 signaling pathway emerged as a critical mediator in this process. In UC, we observed a marked upregulation of IL-17A, CXCL1, IL-6, MMP3, and TNFAIP3, all of which are known to drive inflammatory responses. However, these genes were downregulated in CACRC, which may reflect a shift from an inflammation-dominated environment to a more immunosuppressive tumor microenvironment. This decrease in inflammation-related gene expression in CACRC highlights the complexity of immune regulation during cancer progression. It raises the intriguing possibility that, while chronic inflammation is essential for initiating tumorigenesis, there is a subsequent need to suppress these pathways to allow the tumor to evade immune detection.^{25,26} Moreover, the differential

expression of IL-17 pathway components during UC and CACRC stages underscores the pathway's dualistic role. While IL-17 promotes inflammation in the early stages, aiding the immune response to damage, its downregulation in CACRC could reflect the tumor's adaptation to evade immune surveillance.²⁷ This shift from an inflammatory to an immunosuppressive environment is a hallmark of cancer development. Therefore, targeting IL-17-related pathways might offer a double-edged sword in therapeutic contexts that managing inflammation in UC while also modulating immune evasion in CACRC. In addition to the IL-17 signaling pathway identified in our study, several other signaling cascades have been implicated in the pathogenesis of CACRC. The NF- κ B and STAT3 pathways are known to be persistently activated in chronic inflammation, contributing to epithelial injury, immune cell infiltration, and tumor-promoting cytokine production.²⁸ Moreover, aberrant activation of the Wnt/ β -catenin signaling pathway has been frequently reported in CACRC, driving uncontrolled epithelial proliferation and stemness.²⁹ Notably, TP53 mutations—occurring earlier and more frequently in CACRC than in sporadic CRC—have been associated with DNA damage responses, genomic instability, and impaired immune surveillance.³⁰ Our findings suggest that IL-17 signaling in epithelial cells plays a dynamic, stage-specific role during disease progression. In the ulcerative colitis stage, IL-17 promotes inflammatory responses, chemokine secretion, and tissue remodeling, thereby contributing to chronic tissue injury and epithelial dysfunction. In contrast, the observed decline of IL-17 signaling in CACRC may reflect a transition toward an immune-evasive and tumor-promoting epithelial state. Taken together, our data highlight epithelial IL-17 responsiveness as a critical mediator in the shift from inflammation to malignancy and a potential therapeutic target tailored to different disease stages. These findings underscore the multifactorial and interconnected nature of CACRC development, suggesting that combinatorial targeting of inflammatory and oncogenic pathways may offer more effective therapeutic strategies.

Our study also demonstrated the significant upregulation of C-MYC in CACRC, underscoring its well-established role in promoting cell proliferation and metabolic reprogramming in cancer. The sharp increase in C-MYC expression within epithelial cells in CACRC tissues emphasizes its role as a driver of tumorigenesis.³¹ The metabolic shift observed in CACRC cells, partly driven by C-MYC, suggests that targeting metabolic pathways in CACRC could offer promising therapeutic opportunities.³² Given the well-established role of C-MYC in cell cycle regulation and tumor growth, therapies that specifically disrupt C-MYC signaling could not only impede tumor proliferation but also potentially interfere with cancer cell metabolism, providing a two-pronged approach to CACRC treatment.

In addition to Tregs, B cells also exhibited dynamic changes across disease states. The expansion of cycling plasma B cells in both UC and CACRC, along with their distinct differentiation trajectories, highlights their potential role in shaping immune responses and possibly contributing to antigen presentation during the transition from inflammation to cancer.³³ These findings warrant further investigation into the functional roles of different B cell subtypes in CACRC development and their potential as therapeutic targets.³⁴ The role of plasma B cells in cancer biology is underexplored, and their involvement in CACRC could reveal new dimensions of immune modulation that go beyond traditional adaptive immunity.

A notable aspect of our analysis was the investigation of CNV levels across different disease stages. Cells with high CNV levels were predominantly found in CACRC tissues and were associated with increased genomic instability.^{35,36} This finding supports the notion that genomic instability is a hallmark of cancer, driving both clonal evolution and functional heterogeneity within tumors.³⁷ The correlation between high CNV levels and advanced disease states suggests that targeting genomic instability might provide an avenue for therapeutic intervention aimed at reducing tumor heterogeneity and aggressiveness. By understanding the molecular drivers behind CNV accumulation,³⁸ we could potentially identify biomarkers that not only predict disease progression but also offer therapeutic targets to mitigate the aggressive nature of CACRC.

In summary, this study offers an in-depth single-cell analysis of the progression from UC to CACRC (Figure 8), uncovering significant changes in cellular populations and molecular pathways. The results underscore the intricate relationship between inflammation, immune regulation, and tumor development. Notably, regulatory T cells and plasma B cells emerge as crucial players in modulating immune responses and driving tumor progression, presenting promising targets for potential therapeutic strategies.

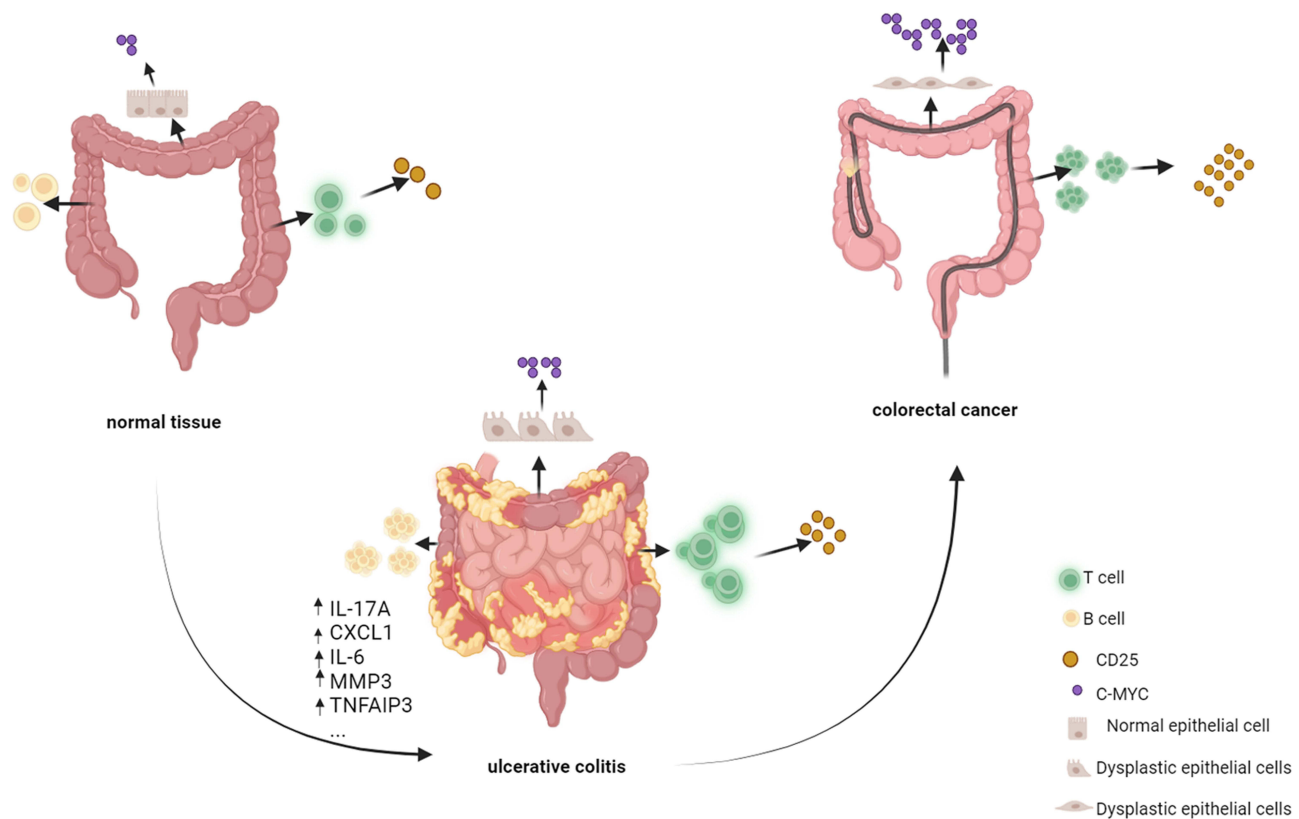


Figure 8 The progression from normal colonic tissue to ulcerative colitis (UC) and colorectal cancer (CACRC). This figure illustrates the stepwise transformation from normal colon tissue to ulcerative colitis and eventually to colorectal cancer. Key cell types involved in this process include T cells (green), B cells (yellow), and dysplastic epithelial cells. The expression of molecular markers, such as C-MYC (purple) and CD25 (Orange), is shown to increase as the disease progresses. In normal tissue, epithelial cells remain healthy with limited immune infiltration. In UC, inflammation and epithelial dysplasia occur, accompanied by an increase in immune cell infiltration and molecular marker expression. In the CACRC stage, dysplastic epithelial cells dominate, with pronounced expression of oncogenic markers. The arrows represent the transition between these stages, highlighting cellular and molecular changes throughout the disease progression.

Data Sharing Statement

The data used and analyzed during this study are available from the corresponding author upon reasonable request.

Ethical Approval

This study was conducted in accordance with the ethical principles outlined in the Declaration of Helsinki and adhered to relevant guidelines and regulations. All experimental protocols were reviewed and approved by the of Anhui medical university the committee on medical ethics (approval code: Quick-PJ 2021-13-23). Informed consent was obtained from all participants involved in the study or their legal guardians prior to participation. The research involving human data was carried out in compliance with applicable guidelines and regulations. The study was approved by Anhui medical university the committee on medical ethics (approval code: Quick-PJ 2021-13-23). Written informed consent was obtained from all participants or their legal guardians prior to inclusion in the study. Written informed consent for the use of tissue samples was obtained from all donors or their legal guardians. The study approval of the first affiliated hospital of Anhui medical university the committee on medical ethics (approval code: Quick-PJ 2021-13-23).

Acknowledgments

We appreciate the support of the National Natural Science Foundation (grant number: 81874063). We are deeply thankful to Mingliang Wang and Xin Xu, for their assistance in guidance and constructive suggestions during this project, which have helped improve the quality of this manuscript.

Author Contributions

All authors made a significant contribution to the work reported, whether that is in the conception, study design, execution, acquisition of data, analysis and interpretation, or in all these areas; took part in drafting, revising or critically reviewing the article; gave final approval of the version to be published; have agreed on the journal to which the article has been submitted; and agree to be accountable for all aspects of the work.

Funding

This research was supported by the National Natural Science Foundation, grant number 81874063.

Disclosure

The authors declare no conflicts of interest in this work.

References

1. Le Berre C, Honap S, Peyrin-Biroulet L. Ulcerative colitis. *Lancet*. 2023;402(571):571–584. doi:10.1016/S0140-6736(23)00966-2
2. Kobayashi T, Siegmund B, Le Berre C, et al. Ulcerative colitis. *Nat Rev Dis Primers*. 2020;6(74). doi:10.1038/s41572-020-0205-x.
3. Agrawal M, Allin KH, Mehandru S, et al. The appendix and ulcerative colitis - an unsolved connection. *Nat Rev Gastroenterol Hepatol*. 2023;20:615. doi:10.1038/s41575-023-00774-3
4. Krugliak CN, Torres J, Rubin DT. What does disease progression look like in ulcerative colitis, and how might it be prevented? *Gastroenterology*. 2022;162:1396. doi:10.1053/j.gastro.2022.01.023
5. Motilva V, Talero E, Calvo J, et al. Intestinal immunomodulation. Role of regulative peptides and promising pharmacological activities. *Curr Pharm Des*. 2008;14(71):71–95. doi:10.2174/138161208783330745
6. Gros B, Kaplan GG. Ulcerative colitis in adults: a review. *JAMA*. 2023;330(951):951. doi:10.1001/jama.2023.15389
7. Guo G, Tan Z, Liu Y, Shi F, She J. The therapeutic potential of stem cell-derived exosomes in the ulcerative colitis and colorectal cancer. *Stem Cell Res Ther*. 2022;13:13138. doi:10.1186/s13287-022-02811-5
8. Faye AS, Holmer AK, Axelrad JE. Cancer in Inflammatory Bowel Disease. *Gastroenterol Clin North Am*. 2022;51:649. doi:10.1016/j.gtc.2022.05.003
9. Liu L, Wang Y, Yu S, et al. Transforming growth factor beta promotes inflammation and tumorigenesis in smad4-deficient intestinal epithelium in a YAP-dependent manner. *Adv Sci*. 2023;10:e2300708. doi:10.1002/adv.202300708
10. Cai J, Sun L, Gonzalez FJ. Gut microbiota-derived bile acids in intestinal immunity, inflammation, and tumorigenesis. *Cell Host Microbe*. 2022;30:289. doi:10.1016/j.chom.2022.02.004
11. Papalexli E, Satija R. Single-cell RNA sequencing to explore immune cell heterogeneity. *Nat Rev Immunol*. 2018;18(35):35–45. doi:10.1038/nri.2017.76
12. Chen Y, Wang H, Yang Q, et al. Single-cell RNA landscape of the osteoimmunology microenvironment in periodontitis. *Theranostics*. 2022;12:1074. doi:10.7150/thno.65694
13. Zhou Y, Yang D, Yang Q, et al. Single-cell RNA landscape of intratumoral heterogeneity and immunosuppressive microenvironment in advanced osteosarcoma. *Nat Commun*. 2020;11:6322. doi:10.1038/s41467-020-20059-6
14. Van de Sande B, Lee JS, Mutasa-Gottgens E, et al. Applications of single-cell RNA sequencing in drug discovery and development. *Nat Rev Drug Discov*. 2023;22:496. doi:10.1038/s41573-023-00688-4
15. Sensi B, Angelico R, Toti L, et al. Mechanism, potential, and concerns of immunotherapy for hepatocellular carcinoma and liver transplantation. *Curr Mol Pharmacol*. 2024;17:e1012161775. doi:10.2174/0118761429310703240823045808
16. Zhu Y, Hu Y, Yang C, et al. Progress of angiogenesis signal pathway and antiangiogenic drugs in nasopharyngeal carcinoma. *Curr Mol Pharmacol*. 2024;17:e1012142005.
17. Liu L, Xie Y, Yang H, et al. HPVTIMER: a shiny web application for tumor immune estimation in human papillomavirus-associated cancers. *Imeta*. 2023;2:e130. doi:10.1002/imt2.130
18. Lin A, Jiang A, Huang L, et al. From chaos to order: optimizing fecal microbiota transplantation for enhanced immune checkpoint inhibitors efficacy. *Gut Microbes*. 2025;17:2452277. doi:10.1080/19490976.2025.2452277
19. Zhang J, Wang Z, Zhang X, et al. Large-scale single-cell and bulk sequencing analyses reveal the prognostic value and immune aspects of CD147 in pan-cancer. *Front Immunol*. 2022;13:810471. doi:10.3389/fimmu.2022.810471
20. Li X, Dai Z, Wu X, et al. The comprehensive analysis identified an autophagy signature for the prognosis and the immunotherapy efficiency prediction in lung adenocarcinoma. *Front Immunol*. 2022;13:749241. doi:10.3389/fimmu.2022.749241
21. Peng S, Lin A, Jiang A, et al. CTLs heterogeneity and plasticity: implications for cancer immunotherapy. *Mol Cancer*. 2024;23(58). doi:10.1186/s12943-024-01972-6.
22. Jia L, Jiang Y, Wu L, et al. Porphyromonas gingivalis aggravates colitis via a gut microbiota-linoleic acid metabolism-Th17/Treg cell balance axis. *Nat Commun*. 2024;15:1617. doi:10.1038/s41467-024-45473-y
23. Shi L, Sun Z, Su W, et al. Treg cell-derived osteopontin promotes microglia-mediated white matter repair after ischemic stroke. *Immunity*. 2021;54:1527. doi:10.1016/j.immuni.2021.04.022
24. Smith PM, Howitt MR, Panikov N, et al. The microbial metabolites, short-chain fatty acids, regulate colonic t reg cell homeostasis. *Science*. 2013;341:569. doi:10.1126/science.1241165
25. Winer H, Rodrigues GOL, Hixon JA, et al. IL-7: comprehensive review. *Cytokine*. 2022;160:156049. doi:10.1016/j.cyto.2022.156049
26. Barata JT, Durum SK, Seddon B. Flip the coin: IL-7 and IL-7R in health and disease. *Nat Immunol*. 2019;20:1584. doi:10.1038/s41590-019-0479-x

27. Lu LL, Xiao S-X, Lin Z-Y, et al. GPC3-IL7-CCL19-CAR-T primes immune microenvironment reconstitution for hepatocellular carcinoma therapy. *Cell Biol Toxicol.* 2023;39:3101. doi:10.1007/s10565-023-09821-w
28. Bragg MA, Breaux WA, M'Koma AE. Inflammatory bowel disease-associated colorectal cancer: translational and transformational risks posed by exogenous free hemoglobin alpha chain, a by-product of extravasated erythrocyte macrophage erythrophagocytosis. *Medicina.* 2023;59:1254
29. Myers JN, Schäffer MW, Korolkova OY, et al. Implications of the colonic deposition of free hemoglobin-alpha chain: a previously unknown tissue by-product in inflammatory bowel disease. *Inflamm Bowel Dis.* 2014;20:1530. doi:10.1097/MIB.000000000000144
30. M'Koma AE, Moses HL, Adunyah SE. Inflammatory bowel disease-associated colorectal cancer: proctocolectomy and mucosectomy do not necessarily eliminate pouch-related cancer incidences. *Int J Colorectal Dis.* 2011;26:533. doi:10.1007/s00384-011-1137-4
31. Ala M. Target c-Myc to treat pancreatic cancer. *Cancer Biol Ther.* 2022;23(34):34–50. doi:10.1080/15384047.2021.2017223
32. Xu Y, Yu Q, Wang P, et al. A selective small-molecule c-myc degrader potently regresses lethal c-myc overexpressing tumors. *Adv Sci.* 2022;9:e2104344. doi:10.1002/advs.202104344
33. Fridman WH, Meylan M, Pupier G, et al. Tertiary lymphoid structures and B cells: an intratumoral immunity cycle. *Immunity.* 2023;56:2254. doi:10.1016/j.immuni.2023.08.009
34. Fahlquist-Hagert C, Wittenborn TR, Terczyńska-Dyla E, et al. Antigen presentation by B cells enables epitope spreading across an MHC barrier. *Nat Commun.* 2023;14:6941. doi:10.1038/s41467-023-42541-7
35. Liang J, Sun G, Pan X, et al. Genomic and transcriptomic features between primary and paired metastatic fumarate hydratase-deficient renal cell carcinoma. *Genome Med.* 2023;15(31). doi:10.1186/s13073-023-01182-7.
36. Porubsky D, Höps W, Ashraf H, et al. Recurrent inversion polymorphisms in humans associate with genetic instability and genomic disorders. *Cell.* 2022;185:1986. doi:10.1016/j.cell.2022.04.017
37. Chai RC, Yan H, An S-Y, et al. Genomic profiling and prognostic factors of H3 K27M -mutant spinal cord diffuse glioma. *Brain Pathol.* 2023;33:e13153. doi:10.1111/bpa.13153
38. Li J, Chen Z, Xiao W, et al. Chromosome instability region analysis and identification of the driver genes of the epithelial ovarian cancer cell lines A2780 and SKOV3. *J Cell Mol Med.* 2023;27:3259. doi:10.1111/jcmm.17893

Journal of Inflammation Research

Publish your work in this journal

The Journal of Inflammation Research is an international, peer-reviewed open-access journal that welcomes laboratory and clinical findings on the molecular basis, cell biology and pharmacology of inflammation including original research, reviews, symposium reports, hypothesis formation and commentaries on: acute/chronic inflammation; mediators of inflammation; cellular processes; molecular mechanisms; pharmacology and novel anti-inflammatory drugs; clinical conditions involving inflammation. The manuscript management system is completely online and includes a very quick and fair peer-review system. Visit <http://www.dovepress.com/testimonials.php> to read real quotes from published authors.

Submit your manuscript here: <https://www.dovepress.com/journal-of-inflammation-research-journal>

Dovepress
Taylor & Francis Group